Acta Montanistica Slovaca
ISSN 1335-1788
actamont.tuke.sk

# Deformation Stability Analysis of Foundation of Taijiao High-speed Railway above the Mined-out Area Affected by Rainfall

*Shuren WANG[1*], Kunpeng SHI[2], Wenxue CHEN[3], Yubo CHEN[4] and Marcin RABE[5]*

**Authors' affiliations and addresses:**
[1] School of Civil Engineering, Henan Polytechnic University, Jiaozuo 454003, China; School of Minerals and Energy Resources Engineering, University of New South Wales, Sydney, NSW 2052, Australia
e-mail: shurenwang@hpu.edu.cn

[2] School of Civil Engineering, Henan Polytechnic University, Jiaozuo 454003, China
e-mail: 444583054@qq.com

[3] Department of Civil & Building Engineering, University of Sherbrooke, Sherbrooke J1K 2R1, Canada
e-mail: Wenxue.chen@usherbrooke.ca

[4] School of Civil Engineering, Henan Polytechnic University, Jiaozuo 454003, China
e-mail: 569079218@qq.com

[5] Faculty of Management and Economics of Services, University of Szczecin, Szczecin, Poland
e-mail: marcin.rabe@wzieu.pl

***Correspondence:**
Shuren WANG, School of Civil Engineering, Henan Polytechnic University, Jiaozuo 454003, China; School of Minerals and Energy Resources Engineering, University of New South Wales, Sydney, NSW 2052, Australia
tel.:+86 15738529570
e-mail: shurenwang@hpu.edu.cn

**Funding information**:
National Natural Science Foundation of China
U1810203
Fundamental Research Funds for the Universities of Henan Province, China
NSFRF200202

**Acknowledgement:**
This work was financially supported by the National Natural Science Foundation of China (U1810203), and the Fundamental Research Funds for the Universities of Henan Province (NSFRF200202), China.

**How to cite this article:**
Wang, S.R., Shi, K.P., Chen, W.X., Chen, Y.B. and Rabe, M. (2022). Study on mechanism of pressure relief and permeability enhancement in soft-hard composite coal seam by directional hydraulic flushing technology. *Acta Montanistica Slovaca,* Volume 27 (2), 553-564.

**DOI:**
https://doi.org/10.46544/AMS.v27i2.20

## Abstract
Aiming to the requirements of potential safety risk control along the high-speed railway, taking the foundation of Taijiao high-speed railway above the mined-out area of Dianshang, China as the engineering background, a mechanical model of composite rock strata of the foundation was established based on the theory of thin plate. Combined with the catastrophe theory, the evaluation system of the foundation stability was constructed. Using the self-developed similar model test and rainfall device, the deformation stability of the foundation under the condition of heavy rainfall and dynamic loading of the high-speed railway was analyzed. Results show that the maximum influence depth of the dynamic loading and heavy rainfall on the foundation is about 20 m, and the further compaction of the foundation cracks is the main factor leading to the subsidence of the foundation above the mined-out area. In addition, the increase of the number of longitudinal tensile cracks in the foundation, which gradually plays a dominant role in the new cracks, shows an exponential growth trend. Being affected by the continuous heavy rainfall, the deformation evolution of the foundation displays four stages: the initial stabilization, the slow deformation, the first sudden-jump, and the secondary sudden-jump stages. Among them, the surface's maximum deformation occurs in the secondary sudden jump stage. The conclusions obtained in this study provide a theoretical basis for the stability evaluation and treatment of the foundation of the high-speed railway above the mined-out area.

## Keywords
Mined-out area, foundation, high-speed railway, rainfall, dynamic loading.

## Introduction

China's high-speed railway will face new challenges in the condition of running well, which means to realize the safe, stable operation and maintenance of high-speed railway passing through the mined-out area (Wang et al., 2021a). However, with the increasing density of China's high-speed railway network, the available land resources are decreasing day by day. Furthermore, some high-speed railways have to pass the mined-out areas. Compared with the ordinary foundation, the foundation of the mined-out area is disturbed by mining, and the damaged foundation is used as the subgrade of the high-speed railway, which will cause a potential safety risk for the long-term operation of the high-speed railway (Helm et al., 2021; Wang et al., 2021b).

In recent years, the high-temperature environment, floods, typhoons, and other extreme weather have occurred frequently. For example, the "7·20" extraordinary rainstorm in Henan province and the "10·5" extraordinary flood in Shanxi province occurred in 2021 in China. Under the influence of the sustained heavy rainfall, the ground subsidence, embankment landslide and instability, and other transport infrastructure damage occurred along the Taijiao high-speed railway, which seriously affected the normal operation of the trains (Raj and Sengupta, 2014; Mandal and Sarkar, 2021; Dutta et al., 2021; Shuyan & Fabus, 2019).

To control the foundation deformation of the high-speed railway in safety, it is of great theoretical significance and practical value to study the deformation stability of the foundation of the high-speed railway under the condition of heavy rainfall and dynamic loading to provide the theoretical basis and technical basis for the safe running of the high-speed railway passing the mined-out area. In addition, the foundation's structural evolution characteristics and cracks extension trend under the action of rainwater is to be studied, which can provide the technical support for the grouting reinforcement of the foundation above the mined-out area.

## State of the art

Studying the deformation control of the foundation of the high-speed railway above the mined-out area is still a relatively new topic, and the related results are in the stage of empirical exploration. Taking the pile group of the Hefei-Fuzhou high-speed railway as the background, Liang et al. (2016) constructed the calculation formula of ultimate bearing capacity and the settlement of the pile group in the mined-out area under the loading of the high-speed railway. Jiang and Wang (2019) established a prediction model for surface subsidence and deformation of the mined-out area under the long-term dynamic loading of a train by field monitoring and numerical simulation results. Wang et al. (2019) analyzed the evolution characteristics of the composite pressure-arch in thin bedrock of overlying strata during shallow coal mining. Since the long-term operation of the high-speed railway made the damaged foundation more prone to settlement, therefore, there was a higher settlement standard for the subgrade of the high-speed railway. Srivastava et al. (2020) used self-potential, and resistivity tomography technology to monitor the abandoned roadway and surface deformation in the mined-out area under the railway, and they established the stability evaluation model of the abandoned mine. Zhang et al. (2021) carried out an indoor physical test for the repeated mining of multiple coal seams. Although they analyzed the deformation characteristics and the cracks evolution of overlying rock during coal mining, they did not quantitatively analyze the influence of the settlement of the foundation on the highway subgrade.

It is the main inducement of geological disasters such as landslides and surface subsidence due to a large amount of rainwater infiltration and erosion. The Green-Ampt model is one of the common methods used to study the problem of rainfall infiltration on a slope. Qin et al. (2016) constructed a rainfall infiltration model suitable for the bedrock layered slope and analyzed the stability of the slope based on the Green-Ampt model. Filho and Fernandes (2019) analyzed the failure mechanism and stability of the landslide based on the field monitoring and test data of the residual soil cutting slope under rainfall conditions. Zhao et al. (2020) built a small-scale similarity model to analyze the deformation and fracture characteristics of the slope under the conditions of mining and rainfall. From the perspective of the overall shear strength of the slope, Vandoorne et al. (2021) improved the Green-Ampt model to evaluate the influence of rainfall on the stability of the accumulative-formation slope (Wang et al., 2016). Guo et al. (2021) proposed a numerical method of unsaturated expansive subgrade considering the rainwater infiltration, and they revealed the failure mode and internal mechanism of the expansive subgrade (Mohamad Ali Ridho and Kaewunruen, 2021). Under the action of rainwater, the mechanical properties of rock and soil change significantly, and the strength decreases significantly, which will break the original relative equilibrium state.

It can provide the theoretical basis and technical support for the foundation treatment to investigate the structural characteristics of the foundation of the mined-out area. Wang et al. (2015) conducted the instability mechanism analysis of the pressure-arch in the coal mining field under different seam dip angles. Based on the monitoring data, Song et al. (2018) analyzed the characteristics of roof collapse in the mined-out area and the deformation evolution of the overlying strata. In addition, the influence of rainfall on the surface deformation and the rock stratum migration in the subsidence area was also discussed. Mondal et al. (2020) Investigated the strata behaviour in the destressed zone of a shallow Indian longwall panel with a hard sandstone cover by using

mine-microseismicity and borehole televiewer data. Shi et al. (2021) analyzed the variation characteristics of the overburden crushing rate and distance from the double-layer goaf roof in the Daliuta mining area by combining numerical analysis with a similar test. The studies mentioned above only focus on the overburden fracture or instability mechanism of the mined-out area under coal mining or rainfall, which was not involving the structural evolution and fracture development of the foundation under the coupling action of rainfall and dynamic loading of the high-speed railway (Martinez-Pagan et al., 2013; Pellicani et al., 2017; Zhao et al., 2018; Piwowarski and Strzalkowski, 2019; Cheng et al., 2021).

Taking the foundation of the Taijiao high-speed railway above the mined-out area of Dianshang, China, as the engineering background, the mechanical model of the foundation was established. Based on the catastrophe theory, the stability evaluation system of the upper strata in the mined-out area was constructed. The dynamic loading of the high-speed railway and the rainfall were simulated through a similar model test. And then, the crack propagation of the foundation was counted, and the structural evolution and subsidence of the foundation were analyzed. The research results not only provide a theoretical basis for the stability evaluation of the foundation but also provide the technical support for the construction of the grouting reinforcement of the foundation of the mined-out area.

The rest of this study is organized as follows. The relevant background and the research methods are described in Section-Materials and Methods. Then the results and discussion are given, and finally, the conclusions are summarized.

## Materials and Methods

### Engineering Background

The TaiJiao high-speed railway passed the mined-out area of the Dianshang coal mine in Shanxi province, China, which was located about 2.3 km northeast of Gaoping city. Coal seam No. 3 was mainly mined, with a buried depth of 67.60-73.70 m and a thickness of 4.20-5.30 m, with an average thickness of 4.85 m. The ratio of mining depth to the thickness is 17.2 < 30 (Limit value), which is a typical shallow mined-out area. The mined-out area of the Dianshang coal mine was about 614,287 $m^2$.

The "10·5" extraordinary flood area spaned the mined-out area, with a long duration, a wide range, and heavy rainfall. Under the action of rainwater erosion, the embankment landslide and surface subsidence of the Taijiao high-speed railway seriously affected its operation safety. After the heavy rainfall, the foundation of the mined-out area was reinforced by grouting to ensure the normal operation of the Taijiao high-speed railway, as shown in Fig. 1.

*(a) Subgrade destruction* *(b) Grouting treatment*

*Fig. 1. Damage and treatment of the subgrade after the heavy rainfall.*

### Theoretical Analysis

The long wall full caving mining method was adopted in the Dianshang coal mine. With the advance of the working face, the overlying strata can be divided into the direct roof, lower strata, and upper strata. As shown in Fig. 2(a), the direct roof was broken, falling and filling the mined-out area. The lower strata would break, rotate and bend. The upper strata showed the characteristics of overall bending and sinking. In addition, the strata maintained a good stratification and integrity movement in the overlying strata in the model test. To study the subsidence of the upper composite strata, a mechanical model of the composite plate in the upper strata was established according to the stress characteristics, as shown in Fig. 2(b).

Assuming the deflection $W(x, y, z)$ of the strata, the equilibrium equation is:

$$D\nabla^4 W = -P(x, y) \tag{1}$$

The *i*, *i*+1 and *i*+2 of the overlying strata were taken as the objects. So, the vertical force acting on the *i*+1 strata is $P_{i+1}(x, y)$, which is:

$$P_{i+1}(x, y) = P_i(x, y) - P_{i+2}(x, y) \tag{2}$$

where, $P_i(x, y)$ and $P_{i+2}(x, y)$ are the forces at the top and bottom of the i+1 strata, respectively.

The distance between the centre of the *i* and *i*+1 strata in the composite strata, namely the interface of the two strata, is $\mathbf{1}/\mathbf{2}(h_i + h_{i+1})$. The deflection difference between the two strata is:

$$W_{i+1} - W_i = \frac{1}{2} P_i \left(\frac{h_i}{E_i} + \frac{h_{i+1}}{E_{i+1}}\right) \tag{3}$$

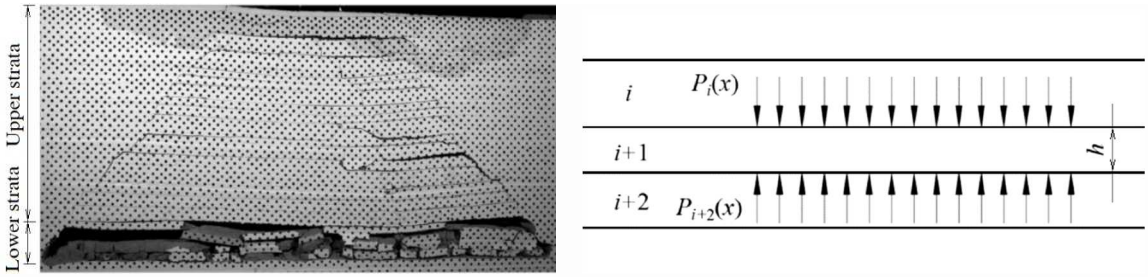


*(a) The movement of overlying strata* *(b) The mechanical model of the upper strata*

*Fig. 2. The movement of the overlying strata and the mechanical model of the upper strata.*

Similarly, the deflection difference between the *i*+1 and *i*+2 strata is as follows:

$$W_{i+2} - W_{i+1} = \frac{1}{2} P_{i+2} \left(\frac{h_{i+1}}{E_{i+1}} + \frac{h_{i+2}}{E_{i+2}}\right) \tag{4}$$

Substituting Eqs. (3) and (4) into Eq. (2), Eq. (5) can be obtained:

$$P_{i+1} = 2E_{i+1}\left[\frac{E_i}{K_i}(W_i - W_{i+1}) + \frac{E_{i+2}}{K_{i+1}}(W_{i+2} - W_{i+1})\right] \tag{5}$$

By substituting Eq. (5) into the Eq. (1), then Eq. (6) can be obtained:

$$\frac{E_{i+1}h_{i+1}^3}{12(1-\mu_{i+1}^2)} \nabla^4 W_{i+1} = 2E_{i+1}\left[\frac{E_i}{K_i}(W_i - W_{i+1}) + \frac{E_{i+2}}{K_{i+1}}(W_{i+2} - W_{i+1})\right] \tag{6}$$

The strength of the foundation weakened after being eroded by rainfall, and the interlayer cracks appeared in the composite beam in the upper strata. As shown in Fig. 3, the mechanic's mode of the composite beam gradually evolved into the supported beam. According to the simply supported beam, considering boundary conditions, lateral force *F*, and upper load *P*(*x*), the deflection w can be expressed as:

$$\omega = y \sin\frac{\pi x}{L} \tag{7}$$

where, *L* is the span of the simply supported beam; *y* is the deflection of the beam midpoint.

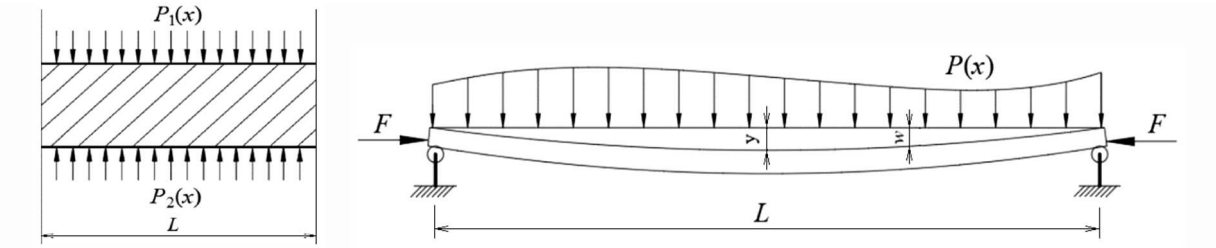


*(a) The composite beam* *(b) The simply supported beam*

*Fig. 3. The mechanical model of the upper strata of the foundation.*

The equilibrium stability of the simply supported beam is studied by the energy method (Ključanin and Manđuka, 2019), and the total potential energy of the system is:

$$U=\frac{EI}{2}\int_0^L\left(\frac{d^2\omega}{dx^2}\right)^2\left(1-\left(\frac{d\omega}{dx}\right)^2\right)^{-1}dx-\left[L-\int_0^L\sqrt{1-\left(\frac{d\omega}{dx}\right)^2}\,dx\right]T-\int_0^L P(x)y\sin\frac{\pi x}{L}dx \tag{8}$$

According to the catastrophe theory (Yin et al., 2015), the stability of the system can be determined by the second variation of the total potential energy:

$$\delta^2U=\frac{\delta^2U}{\delta y^2}(\delta y)^2 \tag{9}$$

As seen from Eq. (9), the second variation and the second-order partial derivative have the same extreme point so that the stability can be determined by the second-order partial derivative of the total potential energy of the system. So, the second-order partial derivative can be obtained:

$$\frac{\delta^2U}{\delta y^2}=\frac{3EI\pi^6}{4L^5}y^2+\frac{\pi^2}{2L}\left(\frac{EI\pi^2}{L^2}-F\right) \tag{10}$$

It can be seen from Eq. (10), when $F\geq\frac{EI\pi^2}{L^2}$, $\frac{\delta^2U}{\delta y^2}\leq 0$, which means that the system is in an unstable state; when $F\leq\frac{EI\pi^2}{L^2}$, $\frac{\delta^2U}{\delta y^2}\geq 0$, which means that the system balance is in a stable state.

**Physical Model Experiment**

**Prepared experiment model.** Taking the foundation of the Taijiao high-speed railway above the mined-out area of Dianshang, China, as the engineering background, the model test was carried out by using a combined multifunctional servo control loading test platform. The platform is 3500 cm long, 64 cm wide, and 2100 cm high. The non-linear loading system is distributed on both sides and the top of the platform, which is used to realize the horizontal direction and the upper loading. The loading range of the hydraulic servo system is 0.1-100 kN, which meets the experimental requirements.

Considering the size of the test platform and the mining conditions of the mined-our areas, according to the similarity theory, the geometric similarity constant $C_l$ of the experimental model was 0.01, the average density of the strata was 2400 kg/m$^3$, and the dry density of the similar materials used in the test was 1600 kg/m$^3$. The similarity constant of the density was $C_\rho$ =1600/2400=0.67, and the acceleration similarity constant was $C_a$ =1. The similarity ratio of the physical quantities of the model was determined by the dimensional analysis method, as shown in Table 1. *C* was a similar constant for the corresponding physical parameter. The sizes of the model were 275 cm long, 30 cm wide, and 93 cm high. The thickness of the coal seam was 4.05 m, and the cutting hole was located at the left boundary of 60 cm. Each mining distance was 5 cm, and the total mining distance was 160 cm (Wu et al., 2018).

*Tab. 1. Similarity ratio of physical parameters in the model.*

| Name | Physical parameters | Relational expression | Similarity ratio |
|---|---|---|---|
| Geometric similarity | Length $l$ | $C_l$ | 0.01 |
| | Displacement $d$ | $C_d = C_l$ | 0.01 |
| Material similarity | Elasticity modulus $E$ | $C_E = C_m C_l^{-1} C_t^{-2}$ | 0.0067 |
| | Density $\rho$ | $C_\rho$ | 0.67 |
| | Compressive strength $\sigma_s$ | $C_{\sigma s}$ | 0.0067 |
| Dynamic similarity | Loading frequency $f$ | $C_f = C_t^{-1}$ | 10 |
| | Accelerator $a$ | $C_a = C_l C_t^{-2}$ | 1 |
| | Time $t$ | $C_t = C_l^{-1/2}$ | 0.1 |

According to the similar ratio of similar materials, fine river sand, lime and gypsum were selected as the main raw materials for the test. The fine river sand below 0.5 mm was used as aggregate, lime and gypsum were used as main cementing materials, and the borax was added as the retarder. Since it is extremely difficult for the materials to follow the strict similar ratio and fully meet the mechanical properties, the uniaxial compressive strength of the similar materials was selected as the main reference index in this test. Some 50 mm × 100 mm standard cylindrical samples were prepared by mixing similar materials with different proportions of 337, 473, 455, and 537. Taking the sample 337 with ratio number as an example, the pressure tester was used at a loading rate of 1 mm/min. After loading for 270 s, the specimen was destroyed with the peak stress of 0.58 MPa. In a similar model, each rock layer corresponds to a similar material ratio, as shown in Table 2. The ratio number means that the first number represents the sand-binder ratio, and the second and third numbers represent the proportion relationship between these two cementing materials. As shown in Tab.2, the value of 337 represents the sand-binder ratio of 3:1. The ratio of lime and gypsum in the cementing materials is 3:7.

The XTDIC full-field strain measurement system was adopted as the monitoring equipment, which was composed of heavy camera support, a pair of high-precision industrial cameras, a camera controller, and a pair of LED fill lights, as shown in Fig. 5(a). The XTDIC test and analysis system combines digital image-related technology and binocular stereo vision technology, the seed points are randomly arranged on the surface of the measured object, and then the deformation trajectory of the seeds is tracked by continuous shooting with high-precision cameras. Finally, the collected images are imported into the calculation module for analysis, which can realize the measurement of three-dimension coordinates, displacement, and strain on the surface of the measured object.

*Tab. 2. Similar materials proportion of the model.*

| Lithology | Proportion number | Compressive strength [MPa] | Actual density [ kg/m³ ] |
|---|---|---|---|
| Subgrade | 537 | 18.80 | 1800 |
| Loess | 573 | 21.30 | 1980 |
| Bedrock | 537 | 22.60 | 2100 |
| Mudstone | 437 | 26.92 | 2250 |
| Sandy mudstone | 473 | 23.88 | 2300 |
| Medium sandstone | 455 | 25.16 | 2400 |
| Siltstone | 337 | 37.80 | 2600 |
| Coal | 573 | 20.00 | 1500 |

**Rainfall and dynamic loading.** Two medical infusion hoses were arranged on the top of a similar model, and the distance between the two hoses was 10 cm. At the same time, a water tank was placed above a similar model, one end of the two hoses was placed in the water tank, and the other end was blocked. The water in the water tank was drained to the subgrade surface under gravity, as shown in Fig. 5(b). The rainwater infiltration

adopted the drip irrigation method, poked a small hole in the medical hose every 2 cm, and used the flow controller to accurately regulate the flow and velocity of water in the hose to simulate the rainfall.

The vibration exciter DH40500 was used as the dynamic loading of the high-speed railway, and the sweep signal generator DH1301 was used as the control device of the vibration exciter, as shown in Fig. 5(c). The exciter would provide a variety of loading waveforms, such as sine wave, triangular wave and rectangular wave, which could meet the requirements of simulating the wheel-rail force generated during the high-speed railway running (Wang et al. 2020).


*(a) XTDIC test* *(b) Rainfall device* *(c) Dynamic loading*

*Fig. 5. The related equipment of the similarity model test.*

## Results and Discussion

### Evolutionary Characteristics Analysis of Overburden Structures

After the layered strata of the similar model were completed and the coal seam was mined-out, the model was consolidated over a period of time, and the strata structure of the mined-out area was constructed. Then, the foundation was preloaded under static load to accelerate the residual settlement of the surface so as to simulate the deformation characteristics of the foundation of the mined-out area under the coupling action of the dynamic loading and rainfall. When the residual of the foundation was stable, the rainwater was infiltrated from the subgrade to the lower foundation through the rainfall device. Under the action of rainwater infiltration and the dynamic loading of the high-speed railway, the evolution characteristics of the foundation of the mind-out area are shown in Fig. 6.

As seen from Fig. 6(a), there are separation cracks with large spacing at a depth of about 15 m from the subgrade surface after the residual of the foundation is stable. The upper strata can be regarded as a composite beam structure. With the rainwater penetrating into the cracks, the hydrostatic pressure constantly increases, resulting in a further expansion in the upper interlayer cracks. In addition, under the action of rainwater erosion, the foundation strength is weakened, the beam of the upper strata gradually appears the layered phenomenon, and the structure of the upper strata gradually evolves from the laminated beam to the simply supported beam, as shown in Fig. 6(b). Due to the loss of the support of the upper beam and the weakening of the strength of the lower beam, the stress of the lower beam exceeds its tensile strength. The deflection of the lower beam gradually increases, a large number of vertical cracks appear in the lower part of the beam, and the opening of the separation cracks between the upper and lower beams further expands. Then, the lower beam appeared to sudden-jump instability failure, and the initial large crack was compressed, as shown in Fig. 6(c). As the rainwater continues to infiltrate, the subsidence of the upper strata is gradually transferred upward. Moreover, the strength of the upper beam is further weakened, which can not bear its self-weight, and then there is another sudden-jump instability failure like the lower beam (Fig. 6(d)).

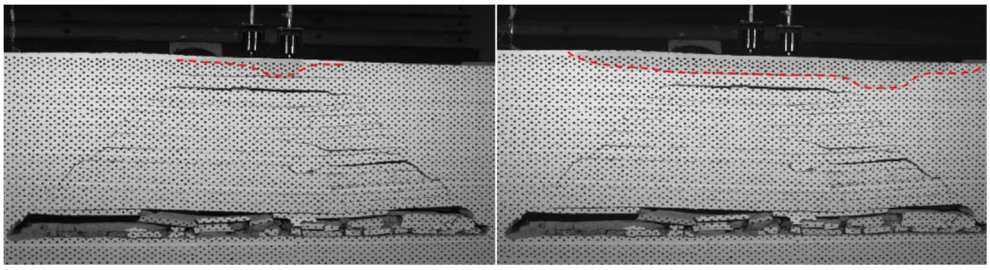

*(a) Initial stabilization stage* *(b) Slow deformation stage*

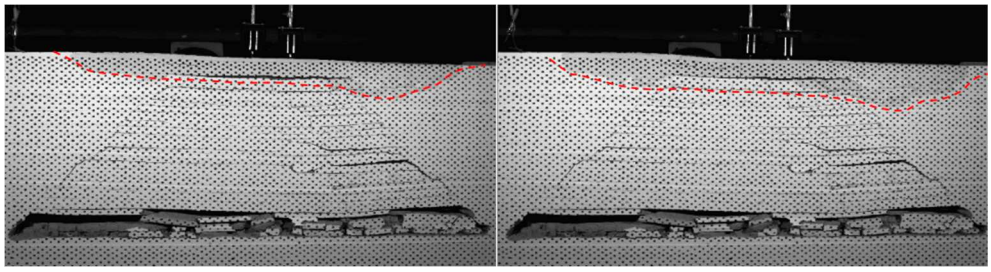

*(c) First sudden-jump stage* *(d) Secondary sudden-jump stage*

*Fig. 6. Structure evolution of the foundation in the mined-out area.*

**Grid Characteristics Analysis of Overburden Fractures in Mined-out Area**

Image J is a public Java-based image processing program with unique advantages in extracting and quantifying cracks in images. By using Image J processing software, the fractured mesh of the overburden in the mined-out area under different rainfall was extracted, as shown in Fig. 7. As seen from Fig. 7, the grids of the overburden fractures are crisscrossed, in which the horizontal interlayer fractures are mainly about 0°, while the longitudinal tensile fractures are mainly about 90°. In addition, the interlayer separation cracks and the vertical penetrating cracks penetrate each other, the overall form shows a stepped shape, and the opening degree of the cracks on both sides of the fracture field is significantly greater than that of the middle bending area.

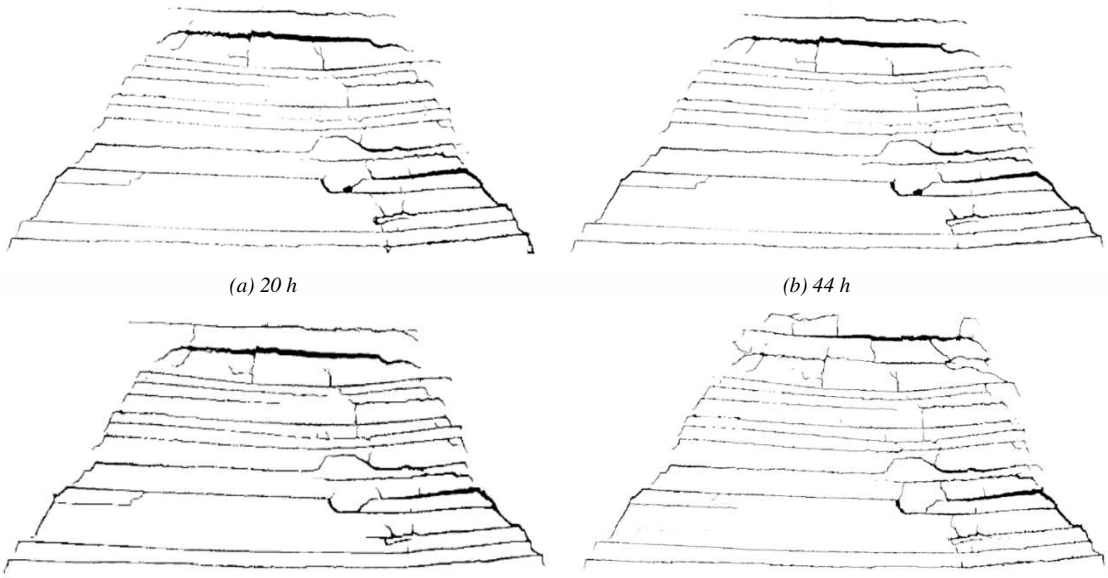

*(a) 20 h* *(b) 44 h*

*(c) 53 h* *(d) 60 h*

*Fig. 7. Variation trend of overburden fissures with rainfall time.*

Under the action of rainwater and the high-speed railway's dynamic loading, the foundation's fractures' evolution characteristics are shown in Fig. 8. As seen from Fig. 8(a), with the increasing of rainfall, the cracks of the foundation gradually close. At the beginning of the rainfall, the strength of the foundation is weakened slowly; therefore, the change in the fissure area is not obvious. While the rain continues to infiltrate, the fissure area of the foundation shrinks sharply, and the interlayer cracks in the middle sinking area are further compressed. The evolution characteristics of the fractures approximately satisfy the quadratic function relationship:

$$S = \mathbf{180} + \mathbf{0.12}t - \mathbf{0.045}t^2 \tag{11}$$

where, $S$ is the fissure area, and $t$ is the rainfall time.

The influence of continuous heavy rainfall results in not only the closure of cracks in the foundation but also the dynamic expansion of cracks in number, as shown in Figs. 8(b) and 8(c). As seen from Fig. 8(b), rainfall's influence on the foundation's transverse interlayer cracks is mainly the extension of cracks, while the new transverse cracks are less affected. With the increase in rainfall, a large number of new longitudinal cracks appear along with the compaction of the middle settlement area in the foundation. The

number of the longitudinal cracks increases from slow to sharp and meets the exponential growth trend, as shown in Fig. 8(c):

$$y = e^{\left(3.96-2.31\times10^{-3}t+4.86\times10^{-5}t\right)} \tag{12}$$

where, $t$ is the rainfall time.

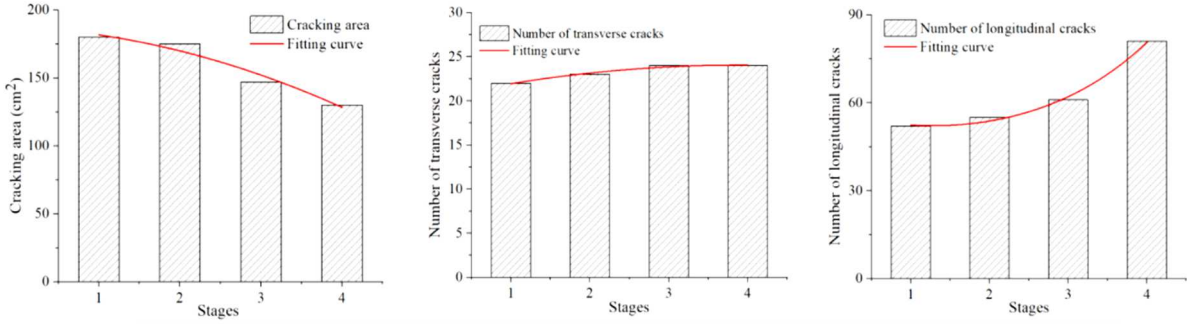


*(a) Cracking area* *(b) Transverse crack* *(c) Longitudinal crack*

*Fig. 8. Cracks evolution in the foundation at different stages.*

**Analysis of Subsidence and Movement of Strata**

A large amount of rainwater seeps into the foundation under the dynamic loading of the high-speed railway, and the most intuitive damage to the foundation is the subsidence, which in turn affects the safe operation of the high-speed railway. Under the action of rainwater erosion, the deformation evolution of the foundation is shown in Fig. 9. As seen from Fig. 9, with the increasing rainfall, the deformation of the foundation under the dynamic loading can be roughly divided into four stages: the initial stabilization stage, the slow deformation stage, the first sudden-jump stage, and the second sudden-jump stage. In the initial stabilization stage, the settlement of the foundation is mainly located at the initial large cracks among the layers and the rotation of the step structure in the lower right-hand corner. As rainwater continues to infiltrate, the deformation of the foundation is concentrated at 5 m to 7.5 m below the surface.

Under the action of the heavy rainfall, the subsidence evolution of the foundation is quantitatively analyzed, as shown in Fig. 10. As seen from Fig. 10, in the initial stage of the rainfall, there is no obvious settlement of the foundation as a whole under the dynamic loading. As the rainfall increases, the small cumulative deformations occur within 20 m depth in the foundation. Then, a sudden deformation occurs in the range of 20 m depth in the foundation, of which the maximum deformation reaches 80 cm, which is located at a depth of 7.5 m. At this point, the subsidence of the surface is about 15 cm. In addition, there is only one sudden-jump deformation at the buried depth of 12.5-20 m, and the deformation is small compared with the overlying rock, only about 10% of that of the overlying rock. As the rainfall continues to increase, the second sudden-jump deformation occurs within 12.5 m depth in the foundation. Different from the first sudden-jump deformation, the deformation of the upper part of the foundation is much larger than that of the lower part. Subsequently, the foundation of the mined-out area gradually tends to be stable without obvious settlement.

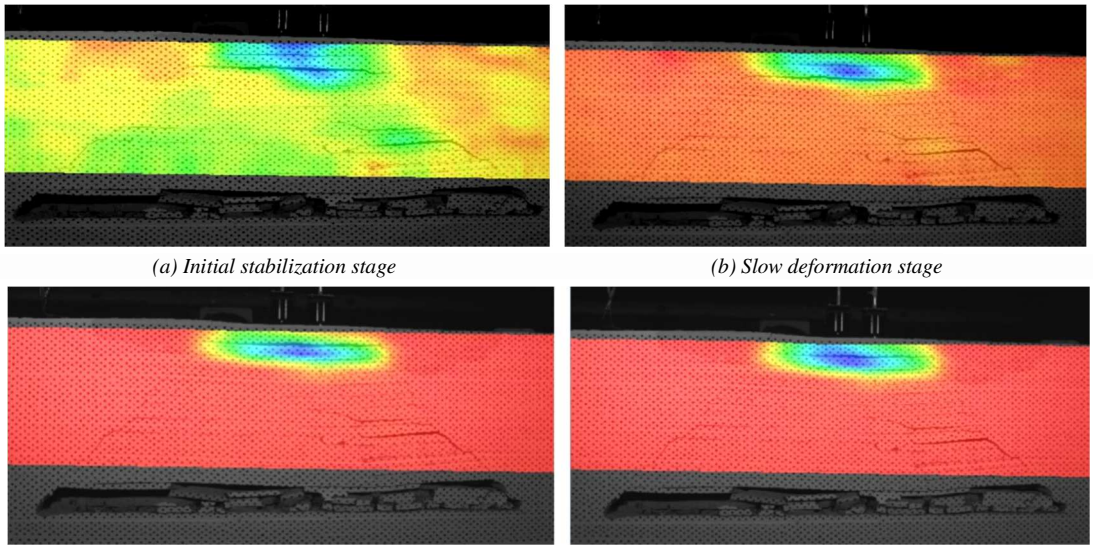

*(a) Initial stabilization stage* *(b) Slow deformation stage*

*(c) First sudden-jump stage* *(d) Second sudden-jump stage*

*Fig. 9. Subsidence evolution of the foundation at different stages.*

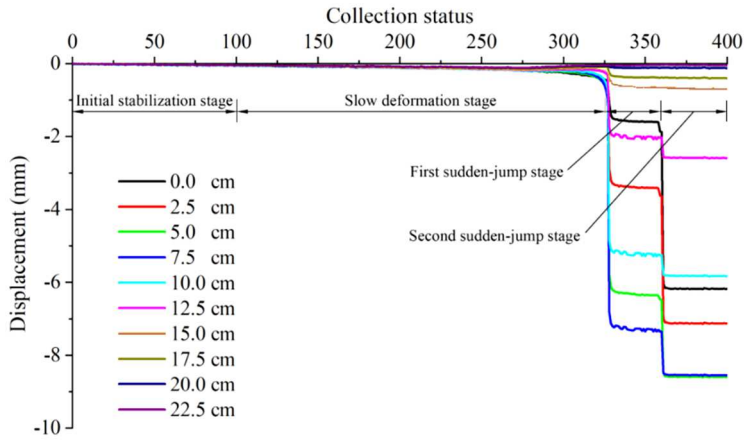


*Fig. 10. Deformation characteristics of foundation with increasing rainfall.*

Under the complex conditions of the rainfall and dynamic loading of the high-speed railway, the distribution characteristics of the final settlement of the foundation are shown in Fig. 11. As seen from Fig. 11(a), the coupling effect of the rainfall and dynamic loading on the settlement of the foundation is concentrated directly above the mined-out area. When a large subsidence area appears on the surface, the maximum influence depth of the rainwater is about 20 m, and the settlement at this position is about 1.0 cm. In addition, the fracture step structure was formed in the near-field of the lower strata during the coal mining. At the same time, the multi-layer rotary extrusion arch structure was formed on the lower right side, resulting in settlement of the foundation offset to the right. As seen from Fig. 11(b), the maximum settlement of the foundation is mainly concentrated in the fracture development area about 7.5 m from the surface, followed by the sedimentation deformation of the surface. When the burial depth exceeds 7.5 m, the settlement deformation of the foundation decreases sharply, roughly satisfying the cubic polynomial:

$$D = -6.89 - 1.02s + 0.16s^2 - 0.004s^3 \tag{13}$$

where, $D$ is the settlement of the foundation, and $s$ is the burial depth.

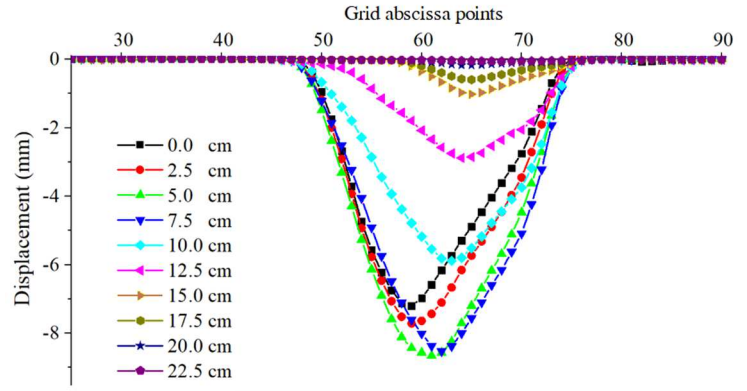


*(a) Subsidence of overlying rock*

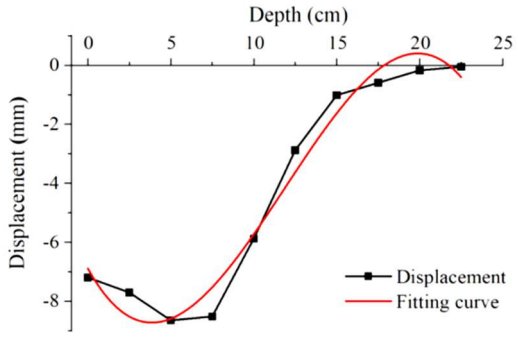


*(b) Deformation curves of the foundation*

*Fig. 11. Final settlement of the foundation under the rainfall.*

## Conclusions

To study the deformation stability of the foundation under the condition of the heavy rainfall, taking the foundation of the mined-out area in the Dianshang coal mine as the engineering background, the mechanical model of the laminated beam of the foundation was established, and the instability criterion of the laminated beam was proposed. By establishing an indoor similarity model of the foundation, the stability of the foundation under the coupling action of the rainfall and dynamic loading of the high-speed railway was analyzed, and the structural evolution mechanism of the foundation was revealed. The main conclusions are obtained as follows:

(1) The mechanical model of the upper strata of the mined-out area was established, and the failure criterion of the composite beam of the foundation was obtained. When the strength of the laminated beam is weakened by rainwater, the delamination occurs, and the laminated beam gradually evolves into the supported beam from bottom to top.

(2) Under the condition of the rainwater erosion, the settlement of the foundation under the dynamic loading of the high-speed railway is caused by the further compaction of the primary cracks in the upper strata, accompanied by the generation of new cracks. The longitudinal fractures are dominant among these cracks and show an exponential growth trend.

(3) Under the coupling action of the rainfall and the dynamic loading, the maximum influence depth in the foundation is about 20 m. The settlement of the foundation can be divided into four stages: initial stability, slow deformation, the first sudden jump, and the second sudden-jump stages.

(4) The influence of the former two stages on the deformation of the foundation is small, and the influence of the second sudden jump is more severe than that of the first sudden jump. The maximum subsidence of the surface occurs in the second sudden-jump stage, and the rainfall is the main inducement factor for the sudden-jump deformation of the foundation.

This study provides a reference for the stability evaluation of the foundation of the mined-out area. However, in order to ensure the safe operation of the high-speed railway, the long-term stability of the foundation of the mined-out area under the more complicated conditions of the high-speed railway is needed to be studied next.

## Reference

Cheng, L., Chang, X., Wang, S.R., Wang, Y.F. and Zhang, M.X. (2021). Effect analysis of bedding plane and fracture distribution on crack propagation process in layered fractured rock mass. Journal of Engineering Science and Technology Review, 14(5). pp. 90-99. DOI: 10.25103/jestr.141.11.

Dutta, K., Wanjari, N. and Misra, A.K. (2021). Study of qualitative stability analysis and rainfall thresholds for possible landslide occurrence: a case study of Sikkim Himalaya. Journal of Taibah University for Science, 15(1). pp. 407-422. DOI: 10.1080/16583655.2021.1984701.

Filho, O.A. and Fernandes, M.A. (2019). Landslide analysis of unsaturated soil slopes based on rainfall and matric suction data. Bulletin of Engineering Geology and the Environment, 78(6). pp. 4167-4185. DOI: 10.1007/s10064-018-1392-5.

Guo, J., Han, J., Zhang, X. and Li, Z.X. (2021). Experimental evaluation of wicking geotextile-stabilized aggregate bases over subgrade under rainfall simulation and cyclic loading. Geotextiles and Geomembranes, 9(6). pp. 1550-1564. DOI: 10.1016/j.geotexmem.2021.07.004.

Helm, P.R., Davie, C.T. and Glendinning, S. (2013). Numerical modelling of shallow abandoned mine working subsidence affecting transport infrastructure. Engineering Geology, 154. pp. 6-19. DOI: 10.1016/j.enggeo.2012.12.003.

Jiang, S. and Wang, Y.M. (2019). Long-term ground settlements over mined-out region induced by railway construction and operation. Sustainability, 11(3). pp. ID 875. DOI: 10.3390/su11030875.

Ključanin, D. and Manđuka, A. (2019). The cantilever beams analysis by the means of the first-order shear deformation and the Euler-Bernoulli theory. Technical Journal, 13(1). pp. 63-67. DOI: 10.31803/tg-20180802210608.

Liang, X., Cheng, Q.G., Wu, J.J., Chen, J.M. (2016). Model test of the group piles foundation of a high-speed railway bridge in mined-out area. Frontiers of Structural and Civil Engineering, 10(4). pp. 488-498. DOI: 10.1007/s11709-016-0338-x.

Mandal, P. and Sarkar, S. (2021). Estimation of rainfall threshold for the early warning of shallow landslides along national highway-10 in Darjeeling Himalayas. Natural Hazards, 105(3). pp. 2455-2480. DOI: 10.1007/s11069-020-04407-9.

Martinez-Pagan, P., Gomez-Ortiz, D., Martin-Crespo, T., Manteca, J.I. and Rosique, M. (2013). The electrical resistivity tomography method in the detection of shallow mining cavities. A case study on the Victoria Cave, Cartagena (SE Spain). Engineering Geology, 156. pp. 1-10. DOI:

10.1016/j.enggeo.2013.01.013.Mohamad Ali Ridho, B.K.A. and Kaewunruen, S. (2021). Failure investigations into interspersed railway tracks exposed to flood and washaway conditions under moving train loads. Engineering Failure Analysis, 129(2). pp. ID 105726. DOI: 10.1016/j.engfailanal.2021.105726.

Mondal, D., Roy, P.N.S. and Kumar, M. (2020). Monitoring the strata behavior in the Destressed Zone of a shallow Indian longwall panel with hard sandstone cover using Mine-Microseismicity and Borehole Televiewer data. Engineering Geology, 271. pp. ID 105593. DOI: 10.1016/j.enggeo.2020.105593.

Pellicani, R., Spilotro, G. and Gutierrez, F. (2017). Susceptibility mapping of instability related to shallow mining cavities in a built-up environment. Engineering Geology, 217. pp. 81-88. DOI: 10.1016/j.enggeo.2016.12.011.

Piwowarski, W. and Strzalkowski, P. (2019). Modeling of discontinuous deformations over shallow post-mining voids in the rock mass. Acta Geodynamica et Geomaterialia, 16(3). pp. 253-256. DOI: 10.13168/AGG.2019.0021.

Qin, X.H., Liu, D.S. and Song, Q.H. (2016). Infiltration model of bedrock laminar slope under heavy rainfall and its stability analysis. Rock and Soil Mechanics, 37(11). pp. 3156-3164. DOI: 10.16285/j.rsm.2016.11.015.

Raj, M. and Sengupta, A. (2014). Rain-triggered slope failure of the railway embankment at Malda, India. ACTA Geotechnica, 9(5). pp. 789-798. DOI: 10.1007/s11440-014-0345-9.

Shi, X. and Zhang, J.X. (2021). Characteristics of overburden failure and fracture evolution in shallow buried working face with large mining height. Sustainability, 13(24). pp. ID 13775. DOI: 10.3390/su132413775.

Shuyan, L., & Fabus, M. (2019). The impact of OFDI reverse technology spillover on China's technological progress: Analysis of provincial panel data. Journal of International Studies, 12(4), 325-336. doi:10.14254/2071-8330.2019/12-4/21

Song, X.G., Chen, C.X. and Xia, K.Z. (2018). Study on ground deformation around collapse zone in Chengchao iron mine. Chinese Journal of Rock Mechanics and Engineering, 37(2). pp. 415-429. DOI: 10.13722/j.cnki.jrme.2017.0916.

Srivastava, S., Pal, S.K. and Kumar, R. (2020). A time-lapse study using self-potential and electrical resistivity tomography methods for mapping of old mine working across railway-tracks in a part of Raniganj coalfield, India. Environmental Earth Sciences, 79(13). pp. ID 332. DOI: 10.1007/s12665-020-09067-3.

Vandoorne, R., Grabe, P.J. and Heymann, G. (2021). Soil suction and temperature measurements in a heavy haul railway formation. Transportation Geotechnics, 31, pp. ID 100675. DOI: 10.1016/j.trgeo.2021.100675.

Wang, D.J., Tang, H.M. and Li, C.D. (2016). Stability analysis of colluvial landslide due to heavy rainfall. Rock and Soil Mechanics, 37(2). pp. 439-445. DOI: 10.16285/j.rsm.2016.02.017.

Wang, S.R., Li, N., Li, C.L., Zou, Z.S. and Chang, X. (2015). Instability mechanism analysis of pressure-arch in coal mining field under different seam dip angles. DYNA, 90(3), pp. 279-284. DOI: 10.6036/7530.

Wang, S.R., Shi, K.P., Zhou, T.H., Zou, Y.F. and Hu, J.C. (2021). Foundation adaptability and subgrade deformation analysis of high-speed railway above the mined-out areas. Journal of Engineering Science and Technology Review, 14(1). pp. 170-177. DOI: 10.25103/jestr.141.20.

Wang, S. R., Shi, K.P., Zou, Y.F., Zou, Z.S., Wang, X.C. and Li, C.L. (2021). Size effect analysis of scale test model for high-speed railway foundation under dynamic loading condition. Tehnicki Vjesnik-Technical Gazette, 28(5). pp. 1615-1625. DOI: 10.17559/TV-20210208101312.

Wang, S.R., Wu, X.G., Zhao, Y.H., Hagan, P. and Cao, C. (2019). Evolution characteristics of composite pressure-arch in thin bedrock of overlying strata during shallow coal mining. International Journal of Applied Mechanics, 11(5). pp. ID 1950030. DOI: 10.1142/S1758825119500303.

Wang, Y., Bai, F., Li, S.H. and Yang, Y.L. (2020). Modelling and dynamic behavior of a vibratory roller for soil compacting based on lumped-parameter method. DYNA, 95(6). pp. 615-621. DOI: 10.6036/9867.

Wu, Q.S., Jiang, L.S., Wu, Q.L., Xue, Y.C. and Gong, B. (2018). A study on the law of overlying strata migration and separation space evolution under hard and thick strata in underground coal mining by si milar simulation. DYNA, 93(2). pp. 615-621. DOI: 10.6036/8678.

Yin, Y.Q., Li, P.E. and Di, Y. (2015). Instability and jumping phenomenon of rock structure. Chinese Journal of Rock Mechanics and Engineering, 34(5): 945-952. DOI: 10.13722/j.cnki.jrme.2014.0275.

Zhao, J.J., Li, J.S. and Ma, Y.T. (2020). Experimental study on failure process of mining landslide induced by rainfall. Journal of China Coal Society, 45(2). pp. 760-769. DOI: 10.13225/j.cnki.jccs.2019.0188.

Zhao, Y.H., Wang, S.R., Zou, Z.S., Ge, L.L. and Cui F. (2018). Instability characteristics of the cracked roof rock beam under shallow mining conditions. International Journal of Mining Science and Technology, 28(3). pp. 437-444. DOI: 10.1016/j.ijmst.2018.03.005.

Zhang, Z.X., Zhang, Y.B., Xu, Y.X., Zhang, Q. and Guo, L.L. (2021). Fracture development and fractal characteristics of overburden rock under repeated mining. Arabian Journal of Geosciences, 14(3), pp. ID 225. DOI: 10.1007/s12517-021-06524-6.